NanoScience and Technology

Roman Krahne · Liberato Manna
Giovanni Morello · Albert Figuerola
Chandramohan George
Sasanka Deka

Physical Properties of Nanorods

Springer

NanoScience and Technology

For further volumes:
http://www.springer.com/series/3705

The series NanoScience and Technology is focused on the fascinating nano-world, mesoscopic physics, analysis with atomic resolution, nano and quantum-effect devices, nanomechanics and atomic-scale processes. All the basic aspects and technology-oriented developments in this emerging discipline are covered by comprehensive and timely books. The series constitutes a survey of the relevant special topics, which are presented by leading experts in the field. These books will appeal to researchers, engineers, and advanced students.

Roman Krahne · Liberato Manna
Giovanni Morello · Albert Figuerola
Chandramohan George
Sasanka Deka

Physical Properties of Nanorods

Springer

Roman Krahne
Chandramohan George
Nanostructures
Istituto Italiano di Tecnologia
Genoa
Italy

Liberato Manna
Nanochemistry
Istituto Italiano di Tecnologia
Genoa
Italy

Giovanni Morello
Nanoscience Institute of CNR
Lecce
Italy

Albert Figuerola
Departament de Química Inorgànica—
Institut de Nanociència i Nanotecnologia
(IN2UB)
Universitat de Barcelona
Barcelona
Spain

Sasanka Deka
Department of Chemistry
University of Delhi
Delhi
India

ISSN 1434-4904
ISBN 978-3-642-36429-7 ISBN 978-3-642-36430-3 (eBook)
DOI 10.1007/978-3-642-36430-3
Springer Heidelberg New York Dordrecht London

Library of Congress Control Number: 2013937190

Printed on acid-free paper

Springer is part of Springer Science+Business Media (www.springer.com)

Preface

Understanding the size and shape dependence of physical properties in nanoscale particles is a fundamental step towards the design, the fabrication, and the assembly of materials and devices with predictable behavior. In recent years, there has been a remarkable advancement in the ability to fabricate shape-controlled nanoparticles, for example rods, wires, and nanoparticles with branched shapes, especially via synthetic approaches in solution. Shape-controlled inorganic nanoparticles are among the most promising candidates as building blocks in nanoscale materials and devices, both because their physical properties are modified considerably compared to those of spherical nanoparticles and because their intrinsic geometry opens many new opportunities for their assembly into organized super-structures. In this book, we have decided to review the physical properties of elongated inorganic nanoparticles, with particular emphasis on the transition in these properties when the shape of the nanoparticles evolves from a sphere to a rod, but we will consider in many cases also nanowires. From the point of view of specific properties and materials, we have decided to cover the optical properties of semiconductors and noble metals, the electrical properties of semiconductors, the magnetic properties of various metals and metal oxides, the catalytic properties of various classes of materials, and the mechanical properties of metals and metal alloys.

Chapter 1 will give an introduction into some basic quantum physics concepts, specifically tailored to the following Chaps. 2 and 3 that are devoted to the optical and electrical properties of semiconductor nanorods. Semiconductor nanocrystals are among the most studied materials in nanoscience nowadays, due to the large number of potential applications employing these materials, for example, in optical devices (lasers [1–3], light emitting diodes [4, 5], photo-detectors [6], solar cells [7–9]), or biological labeling [10, 11], to cite a few. Elongated, rod-shaped semiconductor nanocrystals possess interesting physical properties which depend on their size, aspect ratio, and chemical composition, and these nanoparticles have been proposed as active materials in light emitting devices [12], photocatalysis [13], optically induced light modulation [14], photovoltaics, [7–9, 15] wave-function engineering [16–18], and optical memory elements exploiting the exciton

storage process [19]. More in general, these nanoparticles have been considered as replacement for spherical nanocrystals (the so-called "quantum dots") in all those studies in which the elongated shape could in principle add new or improved properties.

Chapter 4 will deal with optical properties of elongated metal nanocrystals. Metallic nanocrystals have been proposed in a wide range of applications in various fields, among them sensing, biosensing, photodynamic therapy, photovoltaics, optics (light emitting diodes, photo detectors, lasers, imaging techniques beyond the diffraction limit), nano-optics, and nano-electronics (for example plasmonic waveguides) [20–32]. Metal nanostructures can interact strongly with light in the visible and near infrared region of the spectrum, due to the presence of free electrons, which can be promoted both to empty energy levels in the same band or to levels of an empty overlapping band. An incident electromagnetic field can elicit collective oscillations of these free electrons [20–23], which cause a displacement of the electrons from the nuclei, leading to the formation of various possible distributions in the surface charges. This creates Coulomb interactions between positive and negative charges, which induce restoring oscillating forces acting on free electrons. Each type of surface charge distribution is characterized by a collective oscillation mode, also termed as localized surface plasmon resonance. Various factors influence the possible types of SPRs in nanostructures and the frequencies at which they are observed and the shape of metal nanoparticles is certainly one of them. As an example, in rod-shaped nanoparticles the plasmon mode is split into two modes, a longitudinal one and a transverse one. There are many other physical effects connected with an elongated shape which differ from the spherical case, and these will be covered in detail in Chap. 4.

In Chap. 5 we will review the magnetic properties of elongated nanoparticles. Many of the applications of magnetic nanoparticles are in life sciences and biomedicine [33–35]. Superparamagnetism is the term used for describing the absence of coercivity and remanent magnetization in particles that still maintain a considerable amount of polarizable spins under the effect of an external magnetic field [36, 37]. These magnetic nanocrystals, also known as superparamagnets, combine their reduced sizes with their magnetic field responsive character even if no residual magnetization is observed in the absence of an external magnetic field. For this reason they have been proposed as vectors for both in vitro and in vivo transport of different drugs or biomolecules attached to their surfaces, thereby providing selective access to cellular or molecular levels which are inaccessible to conventional therapeutic approaches. In the same way, they can also be used in biodetection and bioseparation techniques since once the target molecule has been attached to the nanocrystals, the application of an external magnetic field will allow their recovery [38, 39]. Iron oxide is clearly the most suitable material for such purposes due to its high chemical stability, biocompatibility, and superparamagnetic properties and iron oxide nanoparticles are being already used in several diagnostic and therapeutic techniques [40].

The achievement of higher coercivity values in particles with reduced size for information storage devices, or faster magnetic responses for smaller biomedical vectors, could be possible if one considers not only the finite size effects of spherical nanocrystals but also the additional phenomena arising from the shape anisotropy of particles such as nanorods. Nanorods or other one-dimensional nanosystems could also be capable of widening the temperature range of applications of a certain magnetic material compared to its bulk form (as will be shown later). The uniaxial shape anisotropy of metallic and oxide nano-objects will probably become a key factor for the development of improved devices. This chapter will also present an overview of various classes of magnetic materials that have been synthesized in nanorod shapes.

Chapter 6 will deal with the catalytic properties of elongated nanoparticles. Today, there is an increasing demand for catalytic materials, in terms of catalytic efficiency, cost of production, specificity, durability, and environmental sustainability [41–44]. This demand is driving research towards the exploitation of new nanoscale catalyst particles, in which the individual components have specific size, shape, exposure of specific reactive surfaces, and suitable combination of materials [45, 46]. Micro- and nanoparticles of various materials have been used as catalysts for many years [47–50], and experimental evidence has been collected so far demonstrating that the catalytic activity of particles is strongly related to their size, and in particular that nanosized particles exhibit increased catalytic activity with respect to larger particles, due to their higher surface to volume ratio [51, 52]. With recent advances in the synthesis of inorganic nanoparticles with controlled size and morphology [53–56], interest has grown towards the understanding of how the catalytic performance of these materials is dependent on shape. In terms of catalytic properties, there are several reasons why an elongated morphology is often preferable over a spherical morphology, and these will be described in Chap. 6, along with several case studies of nanorod-shaped catalysts.

Chapter 7 deals mainly with the mechanical properties of elongated nanoparticles. The miniaturization of micro electromechanical devices and the fabrication of thin films in the electronic industry have started to raise questions already decades ago about the mechanical behavior of confined systems. Early experiments on tensile testing of metal whiskers with micrometer transverse sides have evidenced strengths much higher than the bulk value [57], and recently pure metals and alloys with at least one dimension in the micro- and nanoscale range have been investigated, thanks to advances in the fabrication of new generations of samples suitable for mechanical testing (for example micro pillars prepared by focused ion beam) and in various techniques for studying their stress and deformation properties. Those studies have revealed a marked deviation in the mechanical properties of samples from bulk-like behavior already when their size is of the order of a few micrometers, which is comparable to the length scale of many plasticity mechanisms based on dislocation nucleation and propagation. The increased

strength of single nanocrystals could be useful for applications of these materials as active probes in nano-indentation, scanning probe microscopy, and field emission [58–60], to cite a few. Chapter 7 ends with a paragraph on melting studies on nanorods.

Finally, we conclude this book with some remarks and an outlook on the future directions in this field.

Genoa — Roman Krahne, Liberato Manna, Chandramohan George
Lecce — Giovanni Morello
Barcelona — Albert Figuerola
Delhi — Sasanka Deka

References

1. Chan Y, Caruge JM, Snee PT, Bawendi MG (2004) Multiexcitonic two-state lasing in a CdSe nanocrystal laser. Appl Phys Lett 85(13):2460–2462
2. Klimov VI, Ivanov SA, Nanda J, Achermann M, Bezel I, McGuire JA, Piryatinski A (2007) Single-exciton optical gain in semiconductor nanocrystals. Nature 447(7143):441–446
3. Klimov VI, Mikhailovsky AA, Xu S, Malko A, Hollingsworth JA, Leatherdale CA, Eisler HJ, Bawendi MG (2000) Optical gain and stimulated emission in nanocrystal quantum dots. Science 290(5490):314–317
4. Caruge JM, Halpert JE, Wood V, Bulovic V, Bawendi MG (2008) Colloidal quantum-dot light-emitting diodes with metal-oxide charge transport layers. Nat Phot 2(4):247–250
5. Anikeeva PO, Halpert JE, Bawendi MG, Bulovic V (2009) Quantum dot light-emitting devices with electroluminescence tunable over the entire visible spectrum. Nano Lett 9(7):2532–2536
6. Oertel DC, Bawendi MG, Arango AC, Bulovic V (2005) Photodetectors based on treated CdSe quantum-dot films. Appl Phys Lett 87(21):art. no. 213505
7. Huynh WU, Dittmer JJ, Alivisatos AP (2002) Hybrid nanorod-polymer solar cells. Science 295(5564):2425–2427
8. Kim S, Fisher B, Eisler HJ, Bawendi M (2003) Type-II quantum dots: CdTe/CdSe(core/shell) and CdSe/ZinTe(core/shell) heterostructures. J Am Chem Soc 125(38):11466–11467
9. Gur I, Fromer NA, Geier ML, Alivisatos AP (2005) Air-stable all-inorganic nanocrystal solar cells processed from solution. Science 310(5747):462–465
10. Deka S, Quarta A, Lupo MG, Falqui A, Boninelli S, Giannini C, Morello G, De Giorgi M, Lanzani G, Spinella C, Cingolani R, Pellegrino T, Manna L (2009) CdSe/CdS/ZnS Double shell nanorods with high photoluminescence efficiency and their exploitation as biolabeling probes. J Am Chem Soc 131(8):2948–2958
11. Michalet X, Pinaud F, Lacoste TD, Dahan M, Bruchez MP, Alivisatos AP, Weiss S (2001) Properties of fluorescent semiconductor nanocrystals and their application to biological labeling. Single Mol 2(4):261–276
12. Zhou RH, Chang HC, Protasenko V, Kuno M, Singh AK, Jena D, Xing H (2007) CdSe Nanowires with illumination-enhanced conductivity: Induced dipoles, dielectrophoretic assembly, and field-sensitive emission. J Appl Phys 101(7):art. no. 073704
13. Hewa-Kasakarage NN, El-Khoury PZ, Tarnovsky AN, Kirsanova M, Nemitz I, Nemchinov A, Zamkov M (2010) Ultrafast carrier dynamics in Type II ZnSe/CdS/ZnSe nanobarbells. ACS Nano 4(4):1837–1844

14. Petti L, Rippa M, Fiore A, Manna L, Mormile P (2010) Optically induced light modulation in an hybrid nanocomposite system of inorganic CdSe/CdS nanorods and nematic liquid crystals. Opt Mater 32(9):1011–1016
15. Farva U, Park C (2010) Colloidal synthesis and air-annealing of CdSe nanorods for the applications in hybrid bulk hetero-junction solar cells. Mater Lett 64(13):1415–1417
16. Muller J, Lupton JM, Rogach AL, Feldmann J, Talapin DV, Weller H (2004) Monitoring surface charge movement in single elongated semiconductor nanocrystals. Phys Rev Lett 93(16):art. no. 167402
17. Muller J, Lupton JM, Lagoudakis PG, Schindler F, Koeppe R, Rogach AL, Feldmann J, Talapin DV, Weller H (2005) Wave function engineering in elongated semiconductor nanocrystals with heterogeneous carrier confinement. Nano Lett 5(10):2044–2049
18. Muller J, Lupton JM, Rogach AL, Feldmann J, Talapin DV, Weller H (2005) Monitoring surface charge migration in the spectral dynamics of single CdSe/CdS nanodot/nanorod heterostructures. Phys Rev B 72(20):art. no. 205339
19. Kraus RM, Lagoudakis PG, Rogach AL, Talapin DV, Weller H, Lupton JM, Feldmann J (2007) Room-temperature exciton storage in elongated semiconductor nanocrystals. Phys Rev Lett 98(1):art. no. 017401
20. Klimov V (2004) Semiconductor and metal nanocrystals. Marcel Dekker, New York
21. Noguez C (2005) Optical properties of isolated and supported metal nanoparticles. Opt Mater 27(7):1204–1211
22. Link S, El-Sayed MA (2000) Shape and size dependence of radiative, non-radiative and photothermal properties of gold nanocrystals. Intern Rev Phys Chem 19(3):409–453
23. Perez-Juste J, Pastoriza-Santos I, Liz-Marzan LM, Mulvaney P (2005) Gold nanorods: Synthesis, characterization and applications. Coord Chem Rev 249(17–18):1870–1901
24. Gonzalez AL, Reyes-Esqueda JA, Noguez C (2008) Optical properties of elongated noble metal nanoparticles. J Phys Chem C 112(19):7356–7362
25. Myroshnychenko V, Rodriguez-Fernandez J, Pastoriza-Santos I, Funston AM, Novo C, Mulvaney P, Liz-Marzan LM, de Abajo FJG (2008) Modelling the optical response of gold nanoparticles. Chem Soc Rev 37(9):1792–1805
26. Zhang JZ, Noguez C (2008) Plasmonic optical properties and applications of metal nanostructures. Plasmonics 3(4):127–150
27. Kelly KL, Coronado E, Zhao LL, Schatz GC (2003) The optical properties of metal nanoparticles: The influence of size, shape, and dielectric environment. J Phys Chem B 107(3):668–677
28. Meier M (2007) Plasmonics: Fundamentals and applications. Springer, New York
29. Link S, El-Sayed MA (2003) Optical properties and ultrafast dynamics of metallic nanocrystals. Ann Rev Phys Chem 54:331–366
30. Huang X, Neretina S, El-Sayed MA (2009) Gold nanorods: From synthesis and properties to biological and biomedical applications. Adv Mater 21:4880–4910. doi:10.1002/adma.200802789
31. Liz-Marzan LM (2006) Tailoring surface plasmons through the morphology and assembly of metal nanoparticles. Langmuir 22:32–41. doi:10.1021/la0513353
32. Schwartzberg AM, Olson TY, Talley CE, Zhang JZ (2006) Synthesis, characterization, and tunable optical properties of hollow gold nanospheres. J Phys Chem B 110(40):19935–19944
33. Dobson J (2006) Magnetic nanoparticles for drug delivery. Drug Dev Res 67(1):55–60
34. Park K, Lee S, Kang E, Kim K, Choi K, Kwon IC (2009) New generation of multifunctional nanoparticles for cancer imaging and therapy. Adv Funct Mater 19(10):1553–1566
35. Wilhelm C, Lavialle F, Péchoux C, Tatischeff I, Gazeau F (2008) Intracellular trafficking of magnetic nanoparticles to design multifunctional biovesicles. Small 4(5):577–582
36. Jeong U, Teng X, Wang Y, Yang H, Xia Y (2007) Superparamagnetic colloids: Controlled synthesis and niche applications. Adv Mater 19(1):33–60
37. Lin X-M, Samia ACS (2006) Synthesis, assembly and physical properties of magnetic nanoparticles. J Magn Magn Mater 305(1):100–109

38. Lu A-H, Salabas EL, Schüth F (2007) Magnetic nanoparticles: Synthesis, protection, functionalization, and application. Angew Chem Int Edit 46(8):1222–1244
39. Dave SR, Gao X (2009) Monodisperse magnetic nanoparticles for biodetection, imaging, and drug delivery: A versatile and evolving technology. Wiley Interdisc Rev Nanomed Nanobiotechnol 1(6):583–609
40. Figuerola A, Di Corato R, Manna L, Pellegrino T (2010) From iron oxide nanoparticles towards advanced iron-based inorganic materials designed for biomedical applications. Pharm Res 62(2):126–143
41. Somorjai GA, Park JY (2008) Molecular factors of catalytic selectivity. Angew ChemInt Edit 47(48):9212–9228. doi:10.1002/anie.200803181
42. Min BK, Friend CM (2007) Heterogeneous gold-based catalysis for green chemistry: Low-temperature CO oxidation and propene oxidation. Chem Rev 107(6):2709–2724. doi:10.1021/cr050954d
43. Heitbaum M, Glorius F, Escher I (2006) Asymmetric heterogeneous catalysis. Angew Chem Int Edit 45(29):4732–4762. doi:10.1002/anie.200504212
44. Roucoux A, Schulz J, Patin H (2002) Reduced transition metal colloids: A novel family of reusable catalysts? Chem Rev 102(10):3757–3778. doi:10.1021/cr010350j
45. Norskov JK, Bligaard T, Rossmeisl J, Christensen CH (2009) Towards the computational design of solid catalysts. Nat Chem 1(1):37–46
46. Cuenya BR (2010) Synthesis and catalytic properties of metal nanoparticles: Size, shape, support, composition, and oxidation state effects. Thin Solid Films 518(12):3127–3150. doi:10.1016/j.tsf.2010.01.018
47. Lewis LN (1993) Chemical catalysis by colloids and clusters. Chem Rev 93(8):2693–2730
48. Schmid G (1992) Large clusters and colloids—metals in the embryonic state. Chem Rev 92(8):1709–1727
49. Astruc D, Lu F, Aranzaes JR (2005) Nanoparticles as recyclable catalysts: The frontier between homogeneous and heterogeneous catalysis. Angew Chem Int Edit 44(48):7852–7872. doi:10.1002/anie.200500766
50. Gates BC (1995) Supported metal clusters: Synthesis, structure, and catalysis. Chem Rev 95(3):511–522
51. Wilson OM, Knecht MR, Garcia-Martinez JC, Crooks RM (2006) Effect of Pd nanoparticle size on the catalytic hydrogenation of allyl alcohol. J Am Chem Soc 128(14):4510–4511. doi:10.1021/ja058217m
52. Herzing AA, Kiely CJ, Carley AF, Landon P, Hutchings GJ (2008) Identification of active gold nanoclusters on iron oxide supports for CO oxidation. Science 321(5894):1331–1335. doi:10.1126/science.1159639
53. El-Sayed MA (2004) Small is different: Shape-, size-, and composition-dependent properties of some colloidal semiconductor nanocrystals. Acc Chem Res 37(5):326–333
54. Yin Y, Alivisatos AP (2005) Colloidal nanocrystal synthesis and the organic–inorganic interface. Nature 437(7059):664–670
55. Cozzoli PD, Pellegrino T, Manna L (2006) Synthesis, properties and perspectives of hybrid nanocrystal structures. Chem Soc Rev 35(11):1195–1208
56. Tao AR, Habas S, Yang PD (2008) Shape control of colloidal metal nanocrystals. Small 4(3):310–325
57. Brenner SS (1959) In: Doremus RH, Roberts BW, Turnbull D (eds) Growth and perfection of crystals. Wiley, New York
58. Greer JR, Nix WD (2005) Size dependence of mechanical properties of gold at the sub-micron scale. Appl Phys A Mater Sci Process 80(8):1625–1629
59. Chattopadhyay S, Chen LC, Chen KH (2006) Nanotips: Growth, model, and applications. Crit Rev Solid State Mater Sci 31(1–2):15–53
60. Mazilova TI, Mikhailovskij IM, Ksenofontov VA, Sadanov EV (2009) Field-Ion microscopy of quantum oscillations of linear carbon atomic chains. Nano Lett 9(2):774–778

Acknowledgment

The entire book was derived from an article that we have published in Physics Reports (Roman Krahne, Giovanni Morello, Albert Figuerola, George Chandramohan, Sasanka Deka and Liberato Manna, Physical Properties of Inorganic Elongated Nanoparticles. Physics Reports Volume 501, Issues 3–5, April 2011, Pages 75–221 (2011) doi:10.1016/j.physrep.2011.01.001).

Contents

Chapter 1
Quantum Effects in Confined Systems

In this chapter we give a short introduction to the basic concept of a particle in a box for the discussion of quantum effects in one dimension. This concept will then be expanded to three dimensions in cylindrical coordinates, which are the most adequate to describe rod shaped nanostructures.

A system in which the motion of electrons or other particles (holes, excitons, etc.) is restricted in one or more dimensions, due to some potential profile, is usually referred to as a "low-dimensional" system and shows quantum confinement effects. Due to their dual wave-particle nature, electrons in a solid are treated as particles having an effective mass m^* (accounting for the periodicity of the crystal potential) and a linear momentum arising from their wave-like nature $\vec{p} = \hbar\vec{k}$. Here, $\hbar$ is the Planck's constant divided by 2π, and $\vec{k}$ represents the wavenumber of the associated wave of wavelength $\lambda = 2\pi/k$. The behavior of the electrons is strongly sensitive to the dimensions of the solid in which they move. In the bulk, the infinite extension of the solid is imposed by assigning the so-called periodic boundary conditions, such that the electrons are not affected by the borders of solid in terms of wave function and energy. If however the dimensions of the solid are reduced, the electrons start to "feel" the borders and the assumption of infinite extension of the solid in all the three spatial coordinates does not hold any more. In such a case the system is considered as "quantized".

1.1 One-Dimensional Quantum Box

The simplest way to understand what happens to electrons in the case of a quantized system (in terms of wavefunctions and energies) is to consider the classical textbook case of an electron in a box, which is approached by solving the Schrödinger equation in one dimension (Fig. 1.1) [1]:

$$\frac{d^2\psi}{dx^2} + \frac{2mE}{b^2} = V \quad \text{with} \quad V = \left\{ \begin{array}{ll} 0, & -a/2 < x < a/2 \\ \infty, & x \leq -a/2, x \geq a/2 \end{array} \right\} \tag{1.1}$$

R. Krahne et al., *Physical Properties of Nanorods*,
NanoScience and Technology, DOI: 10.1007/978-3-642-36430-3_1,

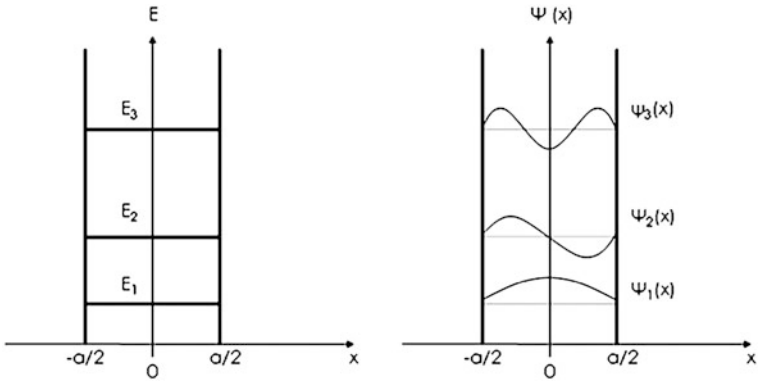

Fig. 1.1 Electrons in a one dimensional quantum box: energy levels and wave functions

We seek for a solution of the form:

$$\psi(x) = Ae^{ikx} + Be^{-ikx} \tag{1.2}$$

Since the potential is infinitely high at the border regions, we need to impose the conditions that the wave functions have to vanish at the borders (i.e. $\psi(-a/2) = 0$ and $\psi(a/2) = 0$, see Fig. 1.1). Upon imposing $\psi(-a/2) = 0$ we obtain:

$$\psi(x) = A\left(e^{ikx} - e^{-ikx}\right) = 2iA\sin(kx) \tag{1.3}$$

and, after substitution in the Schrödinger equation we obtain the following expression for the energy:

$$E = \frac{\hbar^2 k^2}{2m} \tag{1.4}$$

Since $\psi(a/2) = 0$, the following identity must hold:

$$\psi(a/2) = 2iA\sin(ka) = 0 \tag{1.5}$$

The identity is verified only when $ka = n\pi$, with n = 1, 2, 3. Therefore the parameter k is quantized, and the separation between two consecutive values of k is $\Delta k = \Delta n\pi/a$. The quantization energy is expressed as:

$$E_n = \frac{\hbar^2 \pi^2}{2ma^2} n \tag{1.6}$$

In the expression above, the confinement energy is inversely proportional to the square of the size a of the box. As a result, a large value of a corresponds to small spacing of the values in k-space. In the bulk, for example, in which a is practically infinite, there will be a continuous distribution of states in the k-space, in all spatial directions. In a quantum well only one spatial dimension is reduced (down to a few nm), and the electrons can freely move only in a plane, i.e. they behave as a

two-dimensional electron gas (2DEG). The wave numbers have a quasi-continuous distribution along that plane, whereas they are "quantized" along the reduced dimension, following the relation $\Delta k = \Delta n\pi/a$. Several quantum well systems have been fabricated and studied to date (for an overview of some of the pioneering works see for example Refs. [2–6]). If the movement is restricted in two directions, the system is referred to as a "quantum wire", and the electrons can move freely only along the non-reduced dimension. Examples of 1D systems are inorganic semiconductor and metallic nanowires, some organic molecules and carbon nanotubes [7–19]. In the case of quantization in all directions, the electrons possess discrete wavenumbers in the *k*-space and the system is called a "quantum dot". One way to discriminate among the different quantized systems in terms of electronic states is via the density of states function D(E), which represents the number of electronic states in a unitary interval of energy (Fig. 1.2).

In a bulk material (a three-dimensional solid) the density of states follows the well known dependence on the square root of the energy (3D case in Fig. 1.2). This situation corresponds to a quasi-continuous distribution of states for a free-electron gas. In the 2D case (i.e. a two-dimensional solid, 2D case in Fig. 1.2), the global density of states function preserves the quasi-continuous character but becomes a step function framed by the initial square root function. As a consequence, a zero-point energy is introduced and the step spacing is dictated by the energy spacing along the quantized direction. In the 1D case (the "quantum wire") the wave numbers are quantized in two directions and the density of states follows a saw-tooth function (1D case in Fig. 1.2). The latter still describes a quasi-continuous distribution of states, but is now characterized by series of singularities corresponding to the quantization introduced in two dimensions, while the hyperbolas in between two singularities are well described by the reverse of square root of the energy. The 0D sketch of Fig. 1.2 shows what happens in the case of quantization in all three dimensions. The quasi-continuous distribution of states has now collapsed into a series of discrete levels, represented by several Dirac delta functions. In the case of a flat potential with infinite boundaries, the level spacing increases with energy, as described by Eq. (1.6). Such atomic-like structure in the density of states makes these 0D systems fascinating objects, for what concerns both fundamental physics and technological applications [20–25].

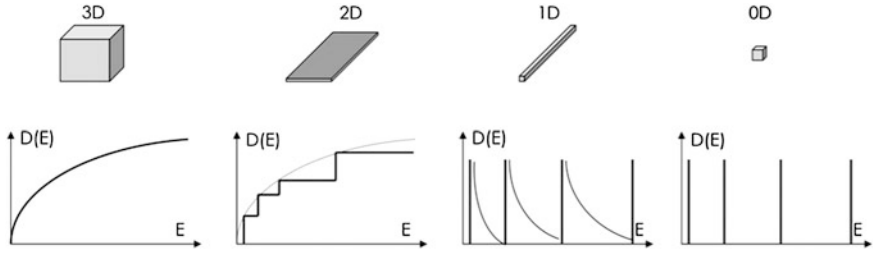

Fig. 1.2 Evolution of the "density of states" function from a bulk (3D solid) to a 2D, 1D and 0D system

1.2 Quantum Confinement in Nanorods

The finite size of the nanorods leads to quantum confinement effects and consequently affects their energy level structure. The optical, electrical, and mechanical properties of the nanorods can be discussed in terms of the related quasi-particles like excitons, electrons, holes, and phonons confined to a cylinder with length L and diameter D. Quantum size effects will have significant impact if the length L, or the diameter D, or both, are of the order or smaller than the Bohr radius associated with the respective quasi-particle. This effective Bohr radius is defined as $a_b = \varepsilon(m/m^*)a_0$, where m and a_0 are the electron mass and Bohr radius, respectively, m^* is the effective mass of the quasi-particle in the bulk material of which the nanocrystal is composed and ε is the dielectric constant of the nanocrystal material in the bulk. The energy spectrum of a quasi-particle confined to a cylinder can be derived from the three-dimensional Schroedinger equation in cylindrical coordinates r, ϕ, and z, and towards that scope we will briefly sketch the solutions in these coordinates. In the simplest case, we can discuss a free particle with effective mass m^* that is confined by infinitely high potential barriers within the cylinder with radius R = D/2 and length L, i.e. the potential V(r) = 0 for r < R and infinite otherwise. In this case independent solutions for the three coordinates can be found of the form [26]:

$$\psi(r,\phi,z) = \rho(r)\Phi(\phi)Z(z) \tag{1.7}$$

Where:

$$\frac{d^2Z}{dz^2} = k_{zk}^2 Z \tag{1.8}$$

$$\frac{d^2\Phi(\phi)}{d\phi^2} = -l^2\Phi \tag{1.9}$$

$$r^2\frac{d^2\rho}{dr^2} + r\frac{d\rho}{dr} + \left(k_{\mathrm{In}}^2 r^2 - l^2\right)\rho = 0 \tag{1.10}$$

With the relation $\kappa^2 = k_{zk}^2 + k_{\mathrm{In}}^2$ for the momentum vector. The solution in z, along the c axis of the rod, is of the form

$$Z(z) = \sin(k_{zk}) = \sin\left(\frac{k\pi}{L}z\right),\ k = 1,2,3,\ldots, \tag{1.11}$$

and has a similar form as the result obtained for a box potential in Eq. (2.5).

In the radial direction we obtain solutions to the Bessel equation:

$$\rho(r) = AJ_l(k_{\mathrm{In}}r) + BY_l(k_{\mathrm{In}}e) \tag{1.12}$$

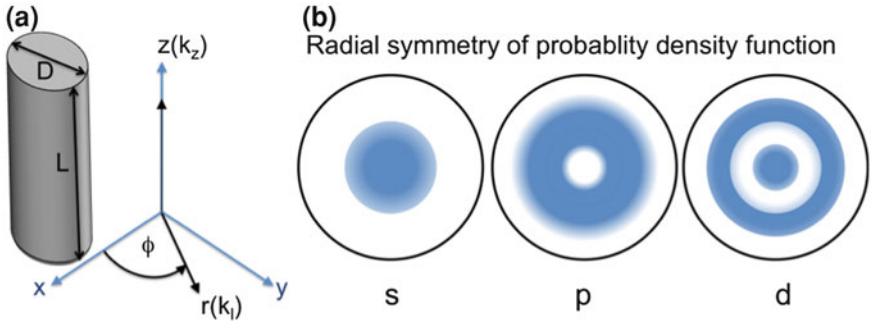

Fig. 1.3 **a** Illustration of the cylindrical coordinates r(kl), z(kz), and f with respect to the rod shape. **b** Schematic illustration of the radial symmetry of the probability density function corresponding to the wave functions in Fig. 1.1

With A and B numbers and J_l and Y_l Bessel functions of the order l of the first and second kind. Due to the radial symmetry this leads to ring like distribution of the wave functions around the z axis of the nanorod as illustrated in Fig. 1.3.

References

1. Yoffe AD (2001) Adv Phys 50(1):1–208
2. Yuan YR, Pudensi MAA, Vawter GA, Merz JL (1985) J Appl Phys 58:397–403
3. Bergman JP, Zhao QX, Holtz PO, Monemar B, Sundaram M, Merz JL, Gossard AC (1991) Time-resolved measurements of the radiative recombination in Gaas/Alxga1-Xas heterostructures. Phys Rev B 43(6):4771–4776
4. Knap W, Borovitskaya E, Shur MS, Hsu L, Walukiewicz W, Frayssinet E, Lorenzini P, Grandjean N, Skierbiszewski C, Prystawko P, Leszczynski M, Grzegory I (2002) Acoustic phonon scattering of two-dimensional electrons in GaN/AlGaN heterostructures. Appl Phys Lett 80(7):1228–1230
5. Katz O, Horn A, Bahir G, Salzman J (2003) Electron mobility in an AlGaN/GaN two-dimensional electron gas I–carrier concentration dependent mobility. IEEE Trans Elec Dev 50(10):2002–2008
6. Mora-Ramos ME, Tutor J, Velasco VR (2006) Interface-phonon-limited two-dimensional mobility in AlGaN/GaN heterostructures. J Appl Phys 100 (12): Article no 123708
7. Hu JT, Odom TW, Lieber CM (1999) Chemistry and physics in one dimension: Synthesis and properties of nanowires and nanotubes. Acc Chem Res 32(5):435–445
8. Cui Y, Lieber CM (2001) Functional nanoscale electronic devices assembled using silicon nanowire building blocks. Science 291(5505):851–853
9. Hakkinen H, Barnett RN, Scherbakov AG, Landman U (2000) Nanowire gold chains: formation mechanisms and conductance. J Phys Chem B 104(39):9063–9066
10. Cobden DH (2001) Molecular electronics–nanowires begin to shine. Nature 409(6816):32–33
11. Cui XD, Primak A, Zarate X, Tomfohr J, Sankey OF, Moore AL, Moore TA, Gust D, Harris G, Lindsay SM (2001) Reproducible measurement of single-molecule conductivity. Science 294(5542):571–574
12. Tans SJ, Devoret MH, Dai HJ, Thess A, Smalley RE, Geerligs LJ, Dekker C (1997) Individual single-wall carbon nanotubes as quantum wires. Nature 386(6624):474–477

13. Saito S (1997) Carbon nanotubes for next-generation electronics devices. Science 278(5335):77–78
14. Yao Z, Postma HWC, Balents L, Dekker C (1999) Carbon nanotube intramolecular junctions. Nature 402(6759):273–276
15. de Heer WA, Chatelain A, Ugarte D (1995) A carbon nanotube field-emission electron source. Science 270(5239):1179–1180
16. Srivastava S, Santos A, Critchley K, Kim KS, Podsiadlo P, Sun K, Lee J, Xu CL, Lilly GD, Glotzer SC, Kotov NA (2010) Light-controlled self-assembly of semiconductor nanoparticles into twisted ribbons. Science 327(5971):1355–1359
17. Duan XF, Huang Y, Agarwal R, Lieber CM (2003) Single-nanowire electrically driven lasers. Nature 421(6920):241–245
18. Oulton RF, Sorger VJ, Zentgraf T, Ma RM, Gladden C, Dai L, Bartal G, Zhang X (2009) Plasmon lasers at deep sub wavelength scale. Nature 461(7264):629–632
19. Baughman RH, Zakhidov AA, de Heer WA (2002) Carbon nanotubes–the route toward applications. Science 297(5582):787–792
20. Bawendi MG, Steigerwald ML, Brus LE (1990) The quantum mechanics of larger semiconductor clusters (quantum dots). Ann Rev Phys Chem 41(V41):477–496
21. Alivisatos AP (1996) Semiconductor clusters, nanocrystals, and quantum dots. Science 271:933–937
22. Alivisatos AP (1998) Electrical studies of semiconductor-nanocrystal colloids. MRS Bull 23(2):18–23
23. Nirmal M, Dabbousi BO, Bawendi MG, Macklin JJ, Trautman JK, Harris TD, Brus LE (1996) Fluorescence intermittency in single cadmium selenide nanocrystals. Nature 383(6603):802–804
24. Konstantatos G, Howard I, Fischer A, Hoogland S, Clifford J, Klem E, Levina L, Sargent EH (2006) Ultrasensitive solution-cast quantum dot photo detectors. Nature 442(7099):180–183
25. Beaulac R, Schneider L, Archer PI, Bacher G, Gamelin DR (2009) Light-induced spontaneous magnetization in doped colloidal quantum dots. Science 325(5943):973–976
26. Eisberg R, Resnick R (1985) Quantum Physics of Atoms, Molecules, Solids, Nuclei, and Particles, 2nd edn. Wiley, New York

Chapter 2
Optical Properties of Semiconductor Nanorods

2.1 Introduction

The optical properties of nanocrystals are dictated by their electronic structure, and we start this section with discussing the behavior of electron–hole pairs, the so called excitons, in confined systems. We then describe the optical peculiarities of semiconductor nanorods by highlighting the main characteristics that distinguish them from the more traditional quantum dots. The first part of this section will focus on the comprehension of the general properties of nanorods made of a single material (henceforth referred to as "homo-structures"), while in the second part of the section we will highlight the properties of nanorods made of sections of different materials (henceforth referred to as "heterostructures"), which have been synthesized by various groups thanks to the latest developments in colloidal nanocrystal synthesis.

2.2 Excitons and Quantum Confinement Regimes

The energy gap of a semiconductor is the energetic separation between the lowest unoccupied electronic state and the highest occupied state at 0 K. The exciton band gap is written as:

$$E_g = E_{g0} + E_q + E_C \tag{2.1}$$

where E_{g0} is the energy gap of the corresponding bulk solid, E_q is the contribution introduced by the quantization and corresponds to the zero-point energy for each system, and E_C is the contribution of the Coulomb attraction between electrons and holes. Their relative contribution is basically related to the degree of confinement to which a system is subjected. In order to better define the role of the quantum confinement on each term of the above expression, we need to introduce the concept of "exciton", which is a "quasi-particle". An exciton is a bound system, composed of an electron (e) and a hole (h) that experience a mutual Coulomb

R. Krahne et al., *Physical Properties of Nanorods*,
NanoScience and Technology, DOI: 10.1007/978-3-642-36430-3_2,

interaction. Here, we will be dealing with a particular type of exciton, in which the e–h distance is much larger than the lattice constant of the crystal in which it is formed, and is usually referred to as a "Wannier-Mott exciton" [1]. One key parameter associated with the exciton is its binding energy, which is defined as:

$$E_b = \frac{\hbar^2}{2\mu r_B^2} \tag{2.2}$$

In the expression above, μ is the reduced mass of the exciton, defined as $1/\mu = (1/m_e + 1/m_h)$, m_e and m_h being the effective masses of electrons and holes, respectively. r_B represents instead the Bohr radius of the exciton, defined as:

$$r_B = \frac{\hbar^2 \varepsilon^2}{\mu e^2} \tag{2.3}$$

with ε being the dielectric constant of the semiconductor. The Bohr radius of the exciton represents its natural spatial extension after its creation (i.e. upon electron–hole pair generation) until its annihilation (upon electron–hole recombination). In bulk semiconductors such radius ranges from a few nm to some tens of nm, depending on the material. The quantization energy is related to the zero-point energy of electrons and holes in the system, and it has always a positive value. In a spherical nanocrystal, for instance, it is defined as [2]:

$$E_q^{e,h} = \frac{\hbar^2 \pi^2}{2m_{e,h} a^2} \tag{2.4}$$

The Coulomb contribution is in general negative, but in some cases it can also be positive (see later in this section). It is proportional to $e^2/\varepsilon^2 a$ and in a spherical quantum dot it can be estimated (as a first approximation) as being equal to [2]:

$$E_C = -1.8 \frac{e^2}{\varepsilon^2 a} \tag{2.5}$$

Therefore, by considering all contributions, the energy gap can be derived from the following expression:

$$E_g = E_{g0} + \frac{\hbar^2 \pi^2}{2m_e a^2} + \frac{\hbar^2 \pi^2}{2m_h a^2} - 1.8 \frac{\hbar^2}{\mu r_B a} \tag{2.6}$$

The optical properties of a semiconductor nanocrystal are dictated by the ratio between the spatial confinement, i.e. the size of the nanocrystal (a), and the Bohr radius r_B of the exciton. Depending on this ratio, three different regimes of quantization can be defined: weak ($a \gg r_B$), intermediate ($a \approx r_B$) and strong ($a < r_B$). In the weak confinement regime, the Coulomb term dominates. Electrons and holes can form the exciton and do not actually "feel" the "restricted" size of the semiconductor. In the intermediate regime, the system can behave in different ways, depending on the ratios between a and the Bohr radii of electrons (r_e) and of the holes (r_h), respectively. In the case that r_h is smaller than r_e the hole will stay

confined at the center of the nanocrystal with the electron orbiting around it, similarly to the case of a donor impurity [3, 4], if a falls in between r_h and r_e. In the strong confinement regime the quantization term dominates over the binding energy of exciton.

2.3 Optical Properties of Nanorods: Overview

The dependence of the energy gap on the size of the nanocrystals is used as a powerful tool for designing materials with well-controlled optical properties. The continuous progress in the development of novel and sophisticated synthesis techniques has opened the possibility to exploit other key parameters for engineering the electronic structure of nanocrystals, such as the shape and the chemical composition. In this respect chemical approaches employing the so-called "high-temperature" thermal reaction of precursors in surfactants have become a popular route to colloidal nanoparticles. This method is so powerful and versatile that a large fraction of nanocrystals discussed in this review have been fabricated in this way. It is also important to note that this method, as many others, yields nanocrystals that are stabilized in the liquid phase by means of a monolayer of organic molecules (i.e. the surfactants) bound to their surface. These molecules need to be considered as a fundamental component of the nanocrystal as they play an important roles in the various physical properties of the nanocrystal, as will be discussed extensively in this review.

Elongated (i.e. rod-shaped) nanocrystals, also known as nanorods, are probably the most studied nanocrystal systems after the spherical ones. Other more complex shapes have been investigated too, but they will not be discussed here [5]. The typical lengths of the nanorods span from tens to some hundreds of nm, while their diameters are generally in the range of a few nm. These nanorods can be considered as intermediate systems between quantum dots and nanowires, since the nanorod length is typically larger than the Bohr radius. Therefore the carriers experience strong confinement only along two dimensions, whereas they can delocalize along the long axis of the rod, giving rise to the so called 1D exciton [6]. This confinement leads to a variety of new properties with respect to spherical nanocrystals, in terms of electronic structure, symmetry, polarization and carrier dynamics.

2.4 Electronic Structure of CdSe Nanorods: A Case Study

Among rod-shaped semiconductor nanocrystals, CdSe nanorods represent probably the most investigated samples, for what concerns both their optical and their electronic properties. Here, we will give an overview of their electronic structure, by highlighting some of the pioneering works in the field (for example those by

Efros et al. [7–9] and by Woggon et al. [10–13]). The concepts discussed here can be considered as of general validity for nanocrystals having hexagonal crystallographic structure and are applicable to nanorods of a wide range diameters and lengths. The starting point is to consider a nanocrystal with dimensions that are much greater than its lattice constant, such that the effective mass approximation [7] is applicable. This condition is practically fulfilled in all cases, since the nanocrystal diameter is hardly smaller than 2–3 nm. In the case of quantum dots, the notation used to name the quantum states follows closely that of an atomic system. We define the total angular momentum J = (L + S) as the sum of the total orbital angular momentum L and the multiplicity term S, the latter accounting for the electron spin. The relative momentum projections are j, l, and s. The electron ground state has s-symmetry and presents a double degeneracy, which is due exclusively to the spin momentum. Thus J = 0 + 1/2, its projections are j = ±1/2, and the state is conventionally indicated as $1S_e$. On the other hand, the first hole level, having a p-symmetry, is fourfold degenerate, having J = 1 + 1/2 = 3/2 (j = 3/2, 1/2, −1/2, −3/2), and is named $1S_{3/2}$. The composition of the two ground states yields the eightfold degenerate exciton ground state $1S_{3/2}1S_e$.

Various effects intervene to lift the degeneracy of the states, namely the internal crystal field, shape effects and the electron–hole exchange interaction. The first effect arises from an intrinsic property of semiconductors that have hexagonal lattice structure and therefore manifests itself in both bulk and nanoscale materials. The second effect results from the deviation from the ideal spherical shape of nanocrystals, while the third accounts for mixing of electron and hole spins. The first two effects can be grouped together, as they arise from the intrinsic asymmetry of the material/nanocrystal (see Fig. 2.1). The intrinsic crystal field produces a first splitting of the valence band, i.e. the lowest hole state, in the so called Kramers doublet, which consists of two doubly degenerate states with j = ±1/2 and j = ±3/2 [7]. Let us define a parameter β as the ratio between the mass of the light hole m_{lh} and the mass of the heavy hole m_{hh} (hence $\beta = m_{lh}/m_{hh}$). The energetic splitting due to the intrinsic crystal field is then expressed as [7]:

$$\Delta_1 = \Delta_{CF} f(\beta) \tag{2.7}$$

where Δ_{CF} is a parameter related to the crystal field (CF) splitting in a crystal with hexagonal structure, contributing to determine the hole ground state as that having |j| = 3/2, while $f(\beta)$ is a function which is unique for each material (see Ref. [7] for details). It is worth to stress that Δ_1 does not depend on the size of nanocrystal. Since $f(\beta)$ is always positive, the lowest hole level is fixed with the heavy-hole state with |j| = 3/2.

In order to take the shape anisotropy into account, let us model an elongated nanocrystal as an axially symmetric ellipsoidal particle (i.e. an ellipsoid with principal axes $a = b < c$), and let us define the ratio of the major to minor axes as $c/b = 1 + \varepsilon$, ε being the ellipticity. The induced splitting in this case is:

$$\Delta_2 = 2u(\beta)E_1(\beta)\varepsilon \tag{2.8}$$

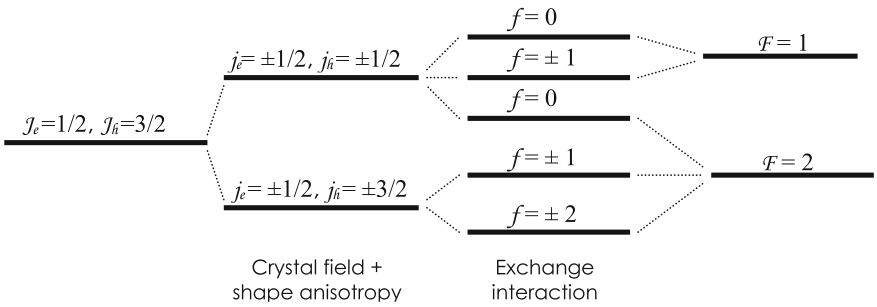

Fig. 2.1 Fine structure splitting of the lowest excitonic states $F = 1$ and $F = 2$ in CdSe nanocrystals due to crystal field, shape anisotropy and exchange interactions

Here, $u(\beta)$ is a dimensionless function associated with the hole-level splitting due to the crystal shape (see Fig. 2.2), for details see Ref. [7]) and $E_1(\beta)$ is the hole ground state energy which can be written as:

$$E_1(\beta) = \frac{\hbar^2 \varphi^2(\beta)}{2m_{hh}a^2} \tag{2.9}$$

where $\varphi^2(\beta)$ is a term related to the spherical Bessel functions and a is related to the nanocrystal size. For quasi spherical nanocrystals $a = (b^2c)^{1/3}$.

Another important point is the trend in the function $u(\beta)$, in particular for what concerns its sign [7]. As shown in Fig. 2.2c $u(\beta)$, reverses its sign past a certain value of β, meaning that for some materials the shape anisotropy induces a negative splitting. Since the global energy splitting is the sum of the single asymmetry contributions $(\Delta_t = \Delta_1 + \Delta_2)$, the final result can reverse the hole ground state between $|j| = 3/2$ and $|j| = 1/2$. A negative Δ_2 is found for example in CdSe nanorods, for which $\beta = 0.28$, and where a possible inversion would depend on the hole ground state energy and on the radius of rods.

We now discuss the excitons, formed by composition of these electron–hole states, which result in two-excitonic fourfold degenerate states, having total angular momentum F = 1 and F = 2 (see right side of Fig. 2.1). The exchange interaction contributes to an increase of the splitting of the remaining states, defining a fine structure for nanocrystals for a series of possible shapes, as depicted in Fig. 2.3 [7].

The relevant quantum number, in this case, is the projection f of the total angular momentum F. The fine structure of the lowest excitonic level is composed by a distribution of states having different values of f: one state with $f = \pm 2$, two states with $f = \pm 1$ (named Upper and Lower, depending on the branch they originate) and two others with f = 0 (Upper and Lower). Only three of them are optically active, namely the states 0^U, $\pm 1^U$ and $\pm 1^L$, whereas the remaining ± 2 and 0^L states are passive [7]. The ± 2 state is optically forbidden because photons cannot have an angular momentum ± 2. The 0^L has zero optical transition probability because of an interference phenomenon between the two indistinguishable states

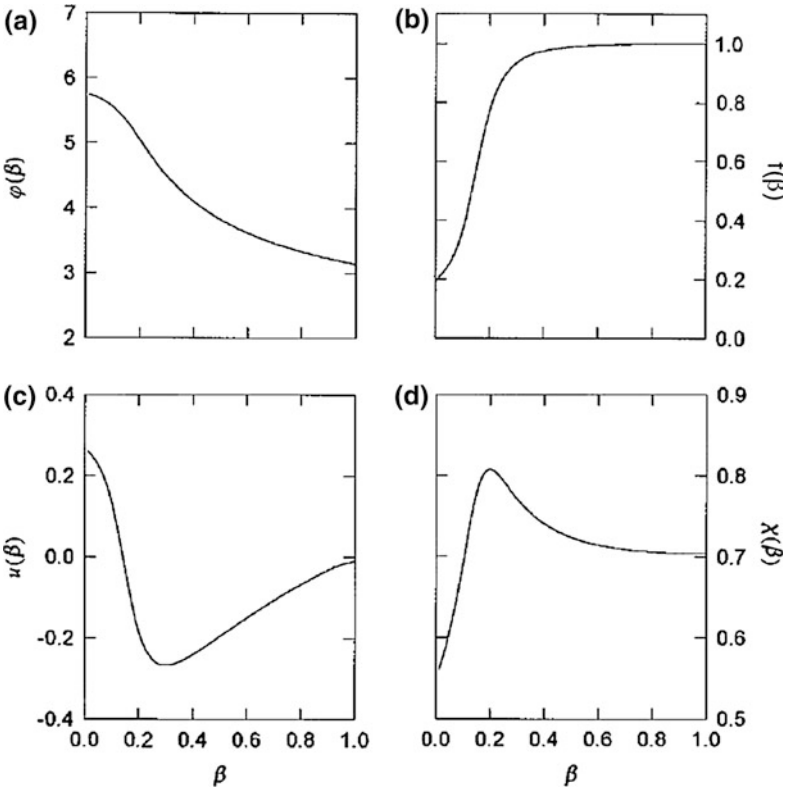

Fig. 2.2 **a** Dependence of the hole ground state function on the light-to-heavy hole ratio mass β. **b–d** Dimensionless functions associated with: **b** hole level splitting due to hexagonal lattice structure, **c** the hole splitting due to the crystal shape asymmetry, **d** the exciton splitting due to the electron–hole-interaction. Taken with permission from Ref. [7]

with zero angular momentum [2], due to the influence of the electron–hole exchange interaction.

The shape of the nanocrystal can have significant influence on which of the above states represents the exciton ground state. For perfectly spherical nanocrystals the ± 2 is the ground state, whereas in prolate nanocrystals an inversion of the ± 2 with the 0^L state can occur, because the state ± 2 originates from the hole state with $|j| = 3/2$, whilst 0^L arises from the state $|j| = 1/2$. When the conditions for the sign change of Δ_t are met, the ground state is inverted. Nanorods can be approximated by axially symmetric prolate ellipsoids with ellipticity ε defined as $\varepsilon = (2r_B/b) - 1$, with b being the ellipsoid diameter and r_B the Bohr radius. In the case of strong lateral confinement $(b < 2r_B)$, the ellipsoids are subject to a possible inversion of the ground state between $\pm$ 2 and 0^L. Following Eq. (2.8), the shape asymmetry can lead to a negative splitting value Δ_2 and then to a negative net splitting $\Delta_t = \Delta_1 + \Delta_2 < 0$, if the ellipsoid radius is smaller than a critical value.

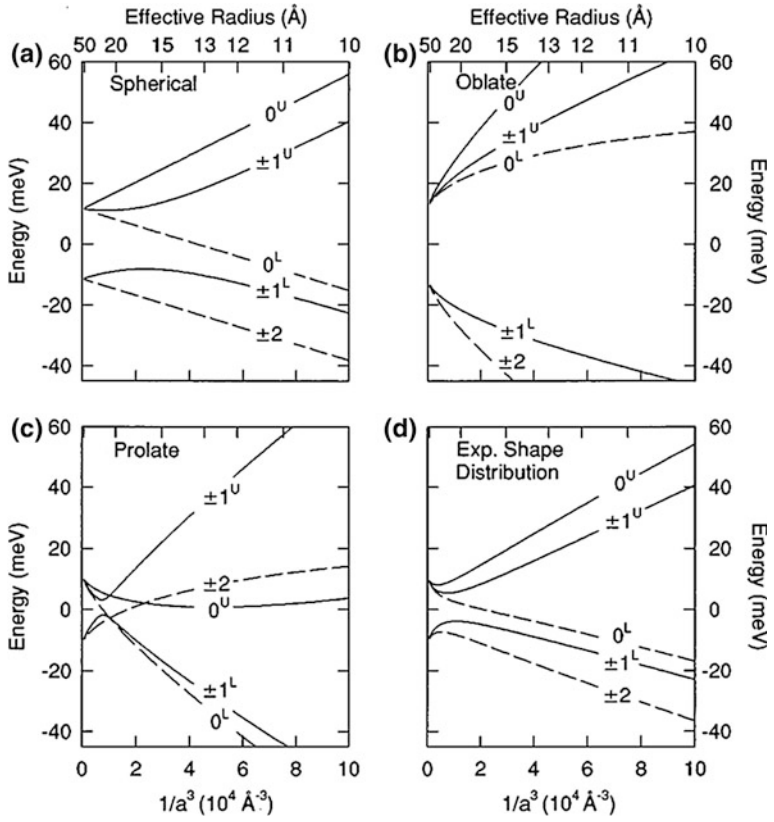

Fig. 2.3 Evolution of the band-edge exciton as a function of the nanocrystal size calculated for four different shapes. Reprinted with permission from Ref. [7]

This can happen because Δ_2 becomes increasingly important in the strong confinement regime, and at some point it would cause the light-hole state with $j = \pm 1/2$ to become the hole ground state. The coupling with the electron state $1S_e$ yields a fourfold degenerate state, with angular momentum 0 (two states) and ± 1. The hole state with $j = \pm 3/2$ yields the second doubly degenerate state with momentum ± 1 and ± 2. In practice, the new lowest exciton level would be the state 0^L and the exciton fine structure resembles that of Fig. 2.3c.

Woggon and co-workers [10] calculated the electronic fine structure of a single CdSe nanorod, taking into account the typical electron–hole exchange interaction for their system (see Fig. 2.4). As expected, by varying the rod radius, two regimes could be identified: for a radius smaller than about 3.7 nm the arrangement of states reflects the well-known fine structure of a spherical nanocrystal, i.e. the lowest energy exciton has angular momentum ± 2. For larger radii on the other hand the exciton ground state has zero angular momentum projection along the major rod axis. This would induce a strongly polarized emission of light, as

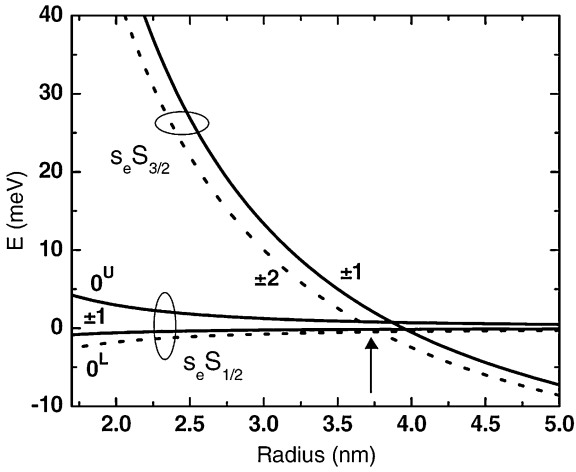

Fig. 2.4 Calculated exciton fine structure of CdSe nanorods. Taken with permission from Ref. [10]

opposed to the quasi-circularly polarized emission predicted for the ±1 excitons. Due to the small energetic separation among these states, thermal population processes give rise to novel phenomena in terms of polarization and carrier relaxation (as discussed later on).

2.5 Relaxation Mechanisms in Nanorods

The carrier mobility in nanorods has a 1D character [6], and this leads to optical properties in nanorods that are remarkably different from those of spherical nanocrystals, among them photoluminescence (PL) lineshape and polarization, radiative and nonradiative transitions, and their dependence on nanocrystal size and temperature. Their understanding represents a first step towards the exploitation of such nanostructures in optical devices. In this section we will discuss the basic optical properties of nanorods in terms of relaxation processes and spectral features, by stressing the differences between nanorods that are entirely made of one material (homo-structures) and those made by sections of different materials (heterostructures). We will distinguish the case of electron–hole relaxation inside the same material from that of relaxation concerning carriers localized in two different materials. In the first case, the possible optical transition is named of type-I, whereas in the second case is of type-II.

2.5.1 One-Dimensional Excitons in Homostructures

In the previous section we have described the fine structure of the ground state exciton in nanorods having a wurtzite structure. Here we will summarize the